processes

MDPI

Article

Mathematical Modeling of Metastatic Cancer Migration through a Remodeling Extracellular Matrix

Yen T. Nguyen Edalgo [1] and Ashlee N. Ford Versypt [1,2,*]

[1] School of Chemical Engineering, Oklahoma State University, Stillwater, OK 74078, USA; yen.t.nguyen@okstate.edu
[2] Stephenson Cancer Center, University of Oklahoma Health Sciences Center, Oklahoma City, OK 73104, USA
* Correspondence: ashleefv@okstate.edu

Received: 22 April 2018 ; Accepted: 14 May 2018; Published: 16 May 2018

Abstract: The spreading of cancer cells, also known as metastasis, is a lethal hallmark in cancer progression and the primary cause of cancer death. Recent cancer research has suggested that the remodeling of collagen fibers in the extracellular matrix (ECM) of the tumor microenvironment facilitates the migration of cancer cells during metastasis. ECM remodeling refers to the following two procedures: the ECM degradation caused by enzyme matrix metalloproteinases and the ECM alignment due to the cross-linking enzyme lysyl oxidase (LOX). Such modifications of ECM collagen fibers result in changes of ECM physical and biomechanical properties that affect cancer cell migration through the ECM. However, the mechanism of such cancer migration through a remodeling ECM remains not well understood. A mathematical model is proposed in this work to better describe and understand cancer migration by means of ECM remodeling. Effects of LOX are considered to enable transport of enzymes and migration of cells through a dynamic, reactive tumor microenvironment that is modulated during cell migration. For validation cases, the results obtained show comparable trends to previously established models. In novel test cases, the model predicts the impact on ECM remodeling and the overall migration of cancer cells due to the inclusion of LOX, which has not yet been included in previous cancer invasion models.

Keywords: computational systems biology; microenvironment; matrix metalloproteinases; lysyl oxidase; degradation; cross-linking

1. Introduction

Every year there are approximately 8.2 million cancer-related deaths worldwide. Metastasis is the primary cause of cancer death. Cancer metastasis occurs when the disease reaches its lethal stage via the uncontrolled spreading of cancer cells to invade a nearby connective tissue and other key organs in the human body. The metastasizing primary tumor cells are not the only agents that drive the progression of metastasis. Instead, metastasis is a systematic process that involves the interaction of cancer cells among a community of various biochemical and cellular factors localized in the tumor microenvironment at both the primary and secondary tumor sites [1]. Many recent cancer-related studies have pointed out that the primary tumor microenvironment contains many important factors that determine whether the primary tumor progresses and proceeds to metastasize or remains dormant, staying a benign tumor [2–6]. In the early stage of metastatic cancer invasion, migration of cancer cells first takes place by breaking away from the primary tumor site and breaching the basement membrane of the tumor. This thin barrier underlying the tumor mass is made up of mostly type IV collagen fibers that separate the tumor from the extracellular matrix (ECM) [7]. After perforating the basement membrane, the escaped cancer cells then must invade the ECM and travel through a meshwork of randomly oriented collagen fibers prior to intravasation into a blood vessel [8]. While maneuvering

through the ECM, the direction and behavior of the migrating cells are greatly influenced by the physical and biomechanical properties of the ECM [9–11].

The ECM is a highly dynamic non-cellular environment present in all tissues of a human body [12]. The ECM consists generally of water, polysaccharides, and proteins. Various types of fibrous proteins are present in the ECM including collagens, elastins, fibronectins, and laminins; among these, collagen is the most abundant and the main structural protein in the ECM [13]. The collagen fibers are constantly being remodeled [10]. The chemical remodeling of collagen fibers results in dynamic changes in the physical, chemical, and biomechanical properties of the ECM [14]. In this article, ECM remodeling refers to the following two processes: (a) ECM degradation caused by enzyme matrix metalloproteinases (MMPs) and (b) ECM alignment due to the cross-linking enzyme lysyl oxidase (LOX). In a pathological condition, like cancer, such changes in the ECM properties facilitate the movement of cells [15]. Via cell–ECM interaction and signaling pathways, these changes elicit cell responses to secrete chemicals like MMPs and LOX to shape the orientation of the ECM from a barrier of randomly oriented fibers into a more propitious fibrous "expressway" for migration [16–18].

The family of MMPs are the most prominent enzymes in ECM remodeling, responsible for proteolytic degradation of the collagen fibers in the ECM [19]. Here, we focus on the collagen fibers residing in the interstitial ECM, which are mostly collagen type I and are degraded by MMP-14, one of the MMP family members secreted by cancer cells [10]. Dysregulation of the activities of MMPs intervenes in almost all cancer types [20] and in the hallmarks of cancer from migration and initial invasion to angiogenesis and metastasis [21]. For simplification, we lump all the family of MMPs together in this work, referring to them collectively as MMP hereafter. Due to its important role as a driving factor for cancer progression, MMP has been and continues to be an appealing and promising target of cancer therapy despite the failure of several clinical trials for MMP inhibitors conducted within the past 30 years [20,22,23].

LOX is a member of the lysyl oxidase family of copper-dependent enzymes. LOX oxidizes primary amine substrates to reactive aldehydes. Via this amine oxidase activity, collagens are cross-linked and aligned in the ECM [24]. Bundles of cross-linked collagen fibers stiffen the matrix and aid the migration of cancer cells via the growth factor signaling pathway [25]. Evidence of thickening and aligned collagen fibers has been observed in areas of active tissue invasion and tumor vasculature [9,16].

Mathematical modeling is a prominent practice in almost all fields of science and engineering in general and in cancer research in particular. Modeling serves as a tool for researchers to formularize and quantitatively understand physical and chemical phenomena observed in reality via the language of mathematics [26]. In the last 20 years or so, many mathematical models of cancer invasion have been established and are constantly being improved upon one another [27–51]. However, no model of cancer invasion has yet considered the enzyme LOX and its promising influence on metastasis via ECM cross-linking. In our mathematical model of metastatic cancer invasion, we not only added a new equation for LOX but also extended the existing models with improved features, showing how LOX affects ECM remodeling and metastatic cancer migration.

In the following sections, we derive and formulate a system of five partial differential equations (PDEs) to describe the local invasion and migration of cancer cells through a remodeling ECM. We also briefly introduce the method used to numerically solve our model in MATLAB (R2017b, MathWorks, Natick, MA, USA, 2017) and detail in Tables 1 and 2 all the parameter values applied in our simulation. We present our results obtained from the numerical simulation and interpret our *in silico* findings from a biological and pathological perspective. We analyze three case studies to highlight the significance of adding the enzyme LOX into the model and the impact from different modes of haptotaxis caused by LOX on the ECM and on the migration of cancer cells. Lastly, we conclude with remarks on the potential usefulness of the proposed model to further clinical understanding of the critical role of ECM remodeling in the early stages of cancer metastasis.

2. Methods

The setting of the model established in this work is an *in silico* metastatic tumor microenvironment (Figure 1). The model aims to unravel the interconnections between the main concepts of metastasis in the ECM: the spreading of cancer cells, the remodeling of collagen fibers, and the reactions kinetics and transport dynamics of the chemicals involved. We start the model time period just after cancer cells have penetrated the basement membrane of the primary tumor (Figure 1A). At this stage, the malignant cancer cells detach away from the primary tumor mass and squeeze through the gaps in the degraded basement membrane. These motile cancer cells proceed to invade the ECM and maneuver their way through a barrier of ECM collagen fibers undergoing remodeling (Figure 1B–D). Such modification of the ECM facilitates the migration of cancer cells via haptotactic sensing and response from cancer cells toward the degraded and cross-linked areas of ECM collagen fibers. Beyond what our model covers, the escaped cancer cells will eventually reach and intravasate nearby blood vessels or invade other connective tissues to travel to other parts of the body and initiate secondary tumors.

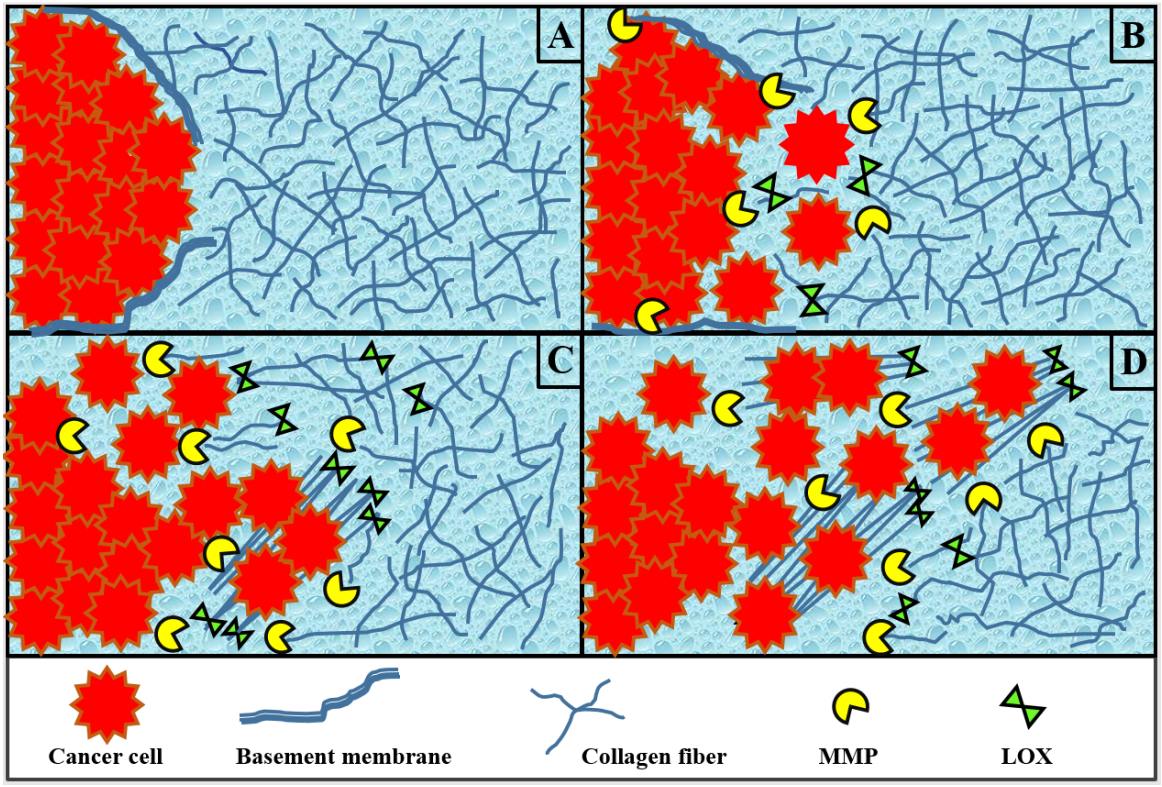

Figure 1. Dynamics in a metastatic tumor microenvironment: (**A**) The basement membrane around the edge of the primary tumor (cluster of cancer cells in red) has already been perforated by cancer cells. The surrounding collagen fibers are randomly oriented in the extracellular matrix (ECM). (**B**) Enzymes metalloproteinase (MMP) and lysyl oxidase (LOX) are secreted by cancer cells to degrade and cross-link collagen fibers. MMP generates spaces for cancer cells to begin detaching away from the primary tumor mass to invade the ECM. (**C**) Meanwhile, aligned and cross-linked collagen fibers form a fibrous pathway along which cancer cells prefer to travel. (**D**) Collagen fibers continue to be cross-linked, aiding the maneuvers of cancer cells further through the matrix.

The model established in this paper is a continuous system of five coupled PDEs describing the dynamics and interaction of cancer cells, collagen fibers, and the enzymes MMP and LOX. Two populations of collagen fibers are considered: those that are oriented randomly and those that have been cross-linked.

2.1. Cancer Cells

The population balance of cancer cells in the system is governed by contributions from three main factors: random diffusion, proliferation, and haptotaxis due to the remodeling ECM collagen fibers:

$$\frac{\partial c}{\partial t} = D_c \frac{\partial^2 c}{\partial x^2} + \gamma c(1 - v_1 c - v_2 f - v_3 f_{cl}) - \frac{\partial}{\partial x}\left[\rho(1 - v_1 c - v_2 f - v_3 f_{cl}) c \frac{\partial f}{\partial x}\right] + g \quad (1)$$

where c is the number of cancer cells per volume of the spatial domain x in one dimension at time t. The first term accounts for the diffusive migration of cells with a constant diffusion coefficient D_c. We assume any nutrient transport supplied to the tumor from nearby blood vessels is unaffected by the remodeling and thus is ignored in our model. The second term is included to account for cell proliferation using a first-order rate expression for c with specific reaction rate γ as an exponential decay function $\gamma = \exp(-x^2/\epsilon)$, where ϵ is an adjustable parameter. The third and fourth terms in the equation implement the haptotaxis effect that directs motility of cancer cells towards the area of remodeling ECM with ρ and ρ_{cl} denoting the haptotaxis parameters for non-cross-linked and cross-linked ECM collagen fibers, respectively. Based on studies on cancer migration using live imaging, cancer cells are prone to move more rapidly on collagen fibers in the collagen enriched area [16,25]. Hence, we assume that the effect of haptotaxis on motility of cancer cells toward the cross-linked area of ECM, f_{cl}, will be stronger than toward the area of degraded ECM that has not yet been cross-linked. We incorporate the logistic growth factor $(1 - v_1 c - v_2 f - v_3 f_{cl})$ in the last three terms of (1) where v_1, v_2, and v_3 are the occupied fractions of one unit volume of physical space by the densities of cancer cells c, regular collagen fibers f, and cross-linked collagen fibers f_{cl}, respectively. The logistic growth factor is implemented to ensure the migration of cancer cells only into space that is not already occupied by the c, f, and f_{cl} present in the system domain [40]. The fourth term g represents the haptotactic migration of cancer cells attracted toward the cross-linked ECM collagen fibers:

$$g = -\frac{\partial}{\partial x}\left[\rho_{cl}(1 - v_1 c - v_2 f - v_3 f_{cl}) c \frac{\partial f_{cl}}{\partial x}\right]. \quad (2)$$

The term g is turned on or off ($g \equiv 0$) in the simulation to investigate the impact of LOX on driving the ECM stiffness via cross-linking and how that influences the overall migration behavior of cancer cells in the system.

2.2. Extracellular Matrix Collagen Fibers

Changes in the morphology and the biochemical and physical properties of the tumor-associated ECM make a substantial impact on regulating cancer progression during metastasis [12]. Since ECM collagen fibers do not diffuse [52] and can be treated as a static structural support network, none of the terms incorporated in the ECM model relate to motility. Instead, the dynamics of ECM is expressed via the remodeling of its collagen fibers due to LOX and MMP. Under disease conditions like cancer, MMP and LOX are known to be dysregulated and often overexpressed, especially in carcinomas. While MMP digests the collagen fibers and generates spaces within the ECM, LOX cross-links and linearizes the fibers, further organizing the matrix of fibers. Although they have different roles in ECM remodeling, both enzymes contribute greatly to transforming ECM from a barrier of fibers into a more navigable fibrous structure that facilitates the migration of cancer cells through the ECM [10,18].

In our model, we include two species to distinguish the structures and functions of the ECM collagen fibers. The randomly oriented collagen fibers that have not been cross-linked are represented by f. The collagen fibers that are cross-linked, linearized, and aligned are denoted by f_{cl}. Assuming a domain of constant volume, the balances for the two collagen fibers species are

$$\frac{\partial f}{\partial t} = -\alpha_f m f + \mu_f(1 - v_1 c - v_2 f - v_3 f_{cl}) - h \quad (3)$$

and

$$\frac{\partial f_{cl}}{\partial t} = -\alpha_f m f_{cl} + h \tag{4}$$

where the first terms in (3) and (4) account for the degradation of collagen fibers of either type by the concentration of MMP m present in the system domain and α_f is the MMP cleavage rate of the collagen fibers. In (3), μ_f is the rate constant for production due to the regular collagen fiber synthesis in the ECM. The logistic growth fraction $(1 - v_1 c - v_2 f - v_3 f_{cl})$ again is incorporated in the source term in (3) to check for the availability of unoccupied space for the normal synthesis of collagen fibers to take place. The term h is included in both (3) and (4) indicating the rate of converting regular collagen fibers into cross-linked fibers. The h term depends on the presence of LOX l and collagen fibers according to

$$h = \beta_f f l \tag{5}$$

where β_f is the reaction rate for cross-linking of collagen fibers by LOX. Like the g term in Equation (1), the h term in (3) and (4) is turned on and off in the simulation depending on the existence of LOX in the system.

2.3. Enzyme MMP

The evolution of the chemical signal MMP in the system is modeled using a reaction-diffusion equation

$$\frac{\partial m}{\partial t} = D_m \frac{\partial^2 m}{\partial x^2} - \alpha_m m + \beta_m c \tag{6}$$

where the first term accounts for MMP diffusion with a constant diffusion coefficient D_m, the second term considers the natural decay of MMP with α_m denoting the MMP decay rate constant, and the third term accounts for the secretion of MMP by cancer cells with a production rate constant β_m. In reality, MMP is secreted by many different types of cells in the malignant tumor microenvironment including cancer-associated fibroblasts (CAFs), inflammatory cells, macrophages, and cancer cells [53]. However, the collagen fibers residing in the interstitial ECM are mostly collagen type I, which is degraded mostly by MMP-1 secreted by CAFs and MMP-14 secreted by cancer cells [10,54]. In the current model, we have not included the existence of CAFs. The secretion of MMP, generally, is considered from cancer cells.

2.4. Enzyme LOX

Similar to that for MMP, the reaction-diffusion equation for LOX is

$$\frac{\partial l}{\partial t} = D_l \frac{\partial^2 l}{\partial x^2} - \alpha_l l + \beta_l c \tag{7}$$

where D_l is the chemical diffusion coefficient of LOX, α_l is the natural decay rate constant for LOX, and β_l is the rate constant for the secretion rate of LOX by cells.

2.5. Nondimensionalization and Parameter Values

To numerically solve the system of PDEs, nondimensionalization is first performed. Nondimensionalization helps establish fewer parameters for efficiently analyzing the system of PDEs. The dimensionless variables are

$$\hat{x} \equiv \frac{x}{L}, \quad \hat{t} \equiv \frac{t}{\tau}, \quad \hat{c} \equiv \frac{c}{c_o}, \quad \hat{f} \equiv \frac{f}{f_o}, \quad \hat{f_{cl}} \equiv \frac{f_{cl}}{f_o}, \quad \hat{m} \equiv \frac{m}{m_o}, \quad \hat{l} \equiv \frac{l}{l_o} \tag{8}$$

where parameters L, τ, c_o, f_o, m_o, and l_o are appropriate reference values for scaling x, t, c, f and f_{cl}, m, and l, respectively. Table 1 summarizes the reference values and parameters that are available from the literature. Considering the early stages of metastatic cancer cell invasion, the length scale L is taken

to be 1 cm but could be in the range of 0.1 to 1 cm. The residence time τ is taken to be 32 h, which is a representative average *in vitro* doubling time for the well-established human cancer cell lines of A549 lung carcinoma cells, U87MG glioma cells, and MCF-7 and MDA-MB 231 breast cancer cells [55–58]. The diffusion coefficient of the cancer cell D_c has been previously determined in an experiment of cell movement by [59]. The diffusion coefficient for the MMP D_m is assumed to be on the order of 10^{-9} cm^2 s^{-1} [60] as is used in [33]. The haptotaxis parameter ρ is taken from [32]. The reference chemical diffusion coefficient D is from [59]. The reference concentration of ECM collagen fiber f_o is in the range of 10^{-11} to 10^{-8} M based on [61]. The lower end value of $f_o = 10^{-11}$, is applied in our model. A value of 0.1×10^{-9} M is taken from [47] as an appropriate reference chemical concentration for both MMP and LOX, m_o and l_o, respectively.

Table 1. Parameter values available from the literature used in the model of metastatic invasion of cancer through remodeling ECM.

Term	Description	Value	Unit	Sources
L	Reference length	1	cm	[33]
τ	Reference time	32	hours	[55–58]
c_o	Reference number of cancer cells per volume	6.7×10^7	cells/cm^3	[33]
f_o	Reference value for f, f_{cl}	10^{-11}	M	[61]
m_o, l_o	Reference value for m, l	0.1×10^{-9}	M	[47]
D_c	Diffusion coefficient of cancer cells	10^{-9}	cm^2/s	[59]
D_m	Diffusion coefficient of MMP	10^{-9}	cm^2/s	[60]
D	Reference chemical diffusion coefficient	10^{-6}	cm^2/s	[59]
ρ	Haptotaxis coefficient toward f	2600	cm^2 M^{-1} s^{-1}	[32]

Introducing the dimensionless quantities defined in (8) into (1)–(7), the model can be written as

$$\begin{aligned}\frac{\partial \hat{c}}{\partial \hat{t}} =& \left(\frac{D_c}{D}\right)\frac{\partial^2 \hat{c}}{\partial \hat{x}^2} + (\gamma\tau)\hat{c}\left(1-(v_1c_o)\hat{c}-(v_2f_o)\hat{f}-(v_3f_o)\hat{f}_{cl}\right) \\ &- \frac{\partial}{\partial \hat{x}}\left[\left(\frac{\rho f_o}{D}\right)\left(1-(v_1c_o)\hat{c}-(v_2f_o)\hat{f}-(v_3f_o)\hat{f}_{cl}\right)\hat{c}\frac{\partial \hat{f}}{\partial \hat{x}}\right] + \hat{g}\end{aligned} \tag{9}$$

$$\hat{g} = -\frac{\partial}{\partial \hat{x}}\left[\left(\frac{\rho_{cl} f_o}{D}\right)\left(1-(v_1c_o)\hat{c}-(v_2f_o)\hat{f}-(v_3f_o)\hat{f}_{cl}\right)\hat{c}\frac{\partial \hat{f}_{cl}}{\partial \hat{x}}\right] \tag{10}$$

$$\frac{\partial \hat{f}}{\partial \hat{t}} = -(\alpha_f\tau m_o)\hat{m}\hat{f} + \left(\frac{\mu_f\tau}{f_o}\right)\left(1-(v_1c_o)\hat{c}-(v_2f_o)\hat{f}-(v_3f_o)\hat{f}_{cl}\right) - \hat{h} \tag{11}$$

$$\frac{\partial \hat{f}_{cl}}{\partial \hat{t}} = -(\alpha_f\tau m_o)\hat{m}\hat{f}_{cl} + \hat{h} \tag{12}$$

$$\hat{h} = (\beta_f\tau l_o)\hat{f}\hat{l} \tag{13}$$

$$\frac{\partial \hat{m}}{\partial \hat{t}} = \left(\frac{D_m}{D}\right)\frac{\partial^2 \hat{m}}{\partial \hat{x}^2} - (\alpha_m\tau)\hat{m} + \left(\frac{\beta_m\tau c_o}{m_o}\right)\hat{c} \tag{14}$$

$$\frac{\partial \hat{l}}{\partial \hat{t}} = \left(\frac{D_l}{D}\right)\frac{\partial^2 \hat{l}}{\partial \hat{x}^2} - (\alpha_l\tau)\hat{l} + \left(\frac{\beta_l\tau c_o}{l_o}\right)\hat{c}. \tag{15}$$

The dimensionless parameters that emerge within parentheses are defined in Table 2. Values for these dimensionless parameters are obtained either through calculation (if sufficient information is provided from literature listed in Table 1, these are labeled as "Calculated") or through approximate values that are reasonable for the model (those with related values obtained from other previous models are listed as "Estimated from" followed by the sources).

Table 2. Dimensionless expression and values of parameters used in MATLAB simulation of metastatic invasion of cancer through a remodeling ECM.

Term	Description	Value	Sources
$\hat{D_c} = D_c/D$	Diffusion coefficient of cell	0.001	Calculated [59]
$\hat{\gamma} = \gamma\tau$	Rate expression for tumor proliferation	$\exp(-\hat{x}^2/\hat{\epsilon})$, $\hat{\epsilon} = 0.001$	Assumed
$\hat{\rho} = \rho f_o \tau/L^2$	Haptotaxis toward f	0.0075	Calculated [59,61]
$\hat{\rho_{cl}} = \rho_{cl} f_o \tau/L^2$	Haptotaxis toward f_{cl}	0.05	Assumed
$\hat{v_1} = v_1 c_o$	Space fraction per unit $\hat{c}$	1	By definition from [40]
$\hat{v_2} = v_2 f_o$	Space fraction per unit $\hat{f}$	1	By definition from [40]
$\hat{v_3} = v_3 f_o$	Space fraction per unit $\hat{f_{cl}}$	1	By definition from [40]
$\hat{\alpha_f} = \alpha_f \tau m_o$	Rate constant for MMP cleavage of f	10	Estimated from [33]
$\hat{\mu_f} = \mu_f \tau/f_o$	Rate constant for production of f	0.15	Estimated from [47]
$\hat{\beta_f} = \beta_f \tau l_o$	Rate constant for LOX remodeling of f	18	Assumed
$\hat{D_m} = D_m/D$	Diffusion of MMP	0.001	Calculated [33,59,60]
$\hat{\alpha_m} = \alpha_m \tau$	Rate constant for decay of MMP	0.001	Estimated from [33,62]
$\hat{\beta_m} = \beta_m c_o \tau/m_o$	Rate constant for secretion of MMP by cells	0.1	Estimated from [33]
$\hat{D_l} = D_l/D$	Diffusion coefficient of LOX	0.002	Assumed
$\hat{\alpha_l} = \alpha_l \tau$	Rate constant for decay of LOX	0.001	Assumed
$\hat{\beta_l} = \beta_l c_o \tau/m_o$	Rate constant for secretion of LOX by cells	0.1	Assumed

2.6. Initial and Boundary Conditions

The initial condition for the cancer cells is set to the same initial condition proposed in several previous cancer invasion mathematical models [35,37,40,47]. The center of the primary tumor mass resides at the left edge of the system domain $\hat{x} = 0$. Initially, it is assumed that a fixed cluster of cancer cells already exists in the system domain from $\hat{x} \in [0, 0.25]$. Additionally, at $\hat{x} = 0.25$ is the edge where the basement membrane of the primary tumor resides before being degraded. The initial distribution of the population density of cancer cells in the system is given by

$$\hat{c}(\hat{x}, 0) = \begin{cases} \exp(\frac{-\hat{x}^2}{\sigma}), & \hat{x} \in [0, 0.25] \\ 0, & \hat{x} \in [0.25, 1] \end{cases} \tag{16}$$

where here σ is a positive constant given a value of 0.01 [33].

Initially, the ECM is a mesh of randomly oriented collagen fibers that are not yet cross-linked:

$$\hat{f}_{cl}(\hat{x}, 0) = 0 \tag{17}$$

To ensure the physical space of the system domain is not congested, the initial condition for the concentration of ECM collagen fibers must satisfy $\hat{c}(\hat{x}, 0) + \hat{f}(\hat{x}, 0) \leq 1$ [40], so

$$\hat{f}(\hat{x}, 0) = 1 - \hat{c}(\hat{x}, 0). \tag{18}$$

We assume that MMP and LOX are absent from the system initially:

$$\hat{m}(\hat{x}, 0) = 0 \tag{19}$$

$$\hat{l}(\hat{x}, 0) = 0. \tag{20}$$

Zero flux boundary conditions for symmetry are imposed on the left edge of the spatial domain ($\hat{x} = 0$) for all components ($\hat{c}$, $\hat{f}$, $\hat{f_{cl}}$, $\hat{m}$, and $\hat{l}$). On the right edge of the spatial domain, it is assumed that there are no cancer cells, cross-linked ECM fibers, MMP, or LOX ($\hat{c}$, $\hat{f_{cl}}$, $\hat{m}$, and $\hat{l}$, respectively).

We assume that there exists a constant amount of non-cross-linked ECM fibers, $\hat{f}$, on the right edge. Hence, the set of boundary conditions imposed on the system is

$$\left.\frac{\partial \hat{c}}{\partial \hat{x}}\right|_{\hat{x}=0} = \left.\frac{\partial \hat{f}}{\partial \hat{x}}\right|_{\hat{x}=0} = \left.\frac{\partial \hat{f}_{cl}}{\partial \hat{x}}\right|_{\hat{x}=0} = \left.\frac{\partial \hat{m}}{\partial \hat{x}}\right|_{\hat{x}=0} = \left.\frac{\partial \hat{l}}{\partial \hat{x}}\right|_{\hat{x}=0} = 0 \tag{21}$$

$$\hat{c}(1,\hat{t}) = \hat{f}_{cl}(1,\hat{t}) = \hat{m}(1,\hat{t}) = \hat{l}(1,\hat{t}) = 0 \tag{22}$$

$$\hat{f}(1,\hat{t}) = 1. \tag{23}$$

2.7. Numerical Methods and Code Repository

The system of coupled PDEs (9)–(23) in this paper is numerically solved in the domain $\Omega = [0,1] \times (0,20]$ utilizing the `pdepe` function, an internal PDE solver in MATLAB that discretizes the equations in space to obtain a system of ordinary differential equations in time that is then solved along the discrete grid points. This function can handle solving initial-boundary value problems for systems of parabolic and elliptic PDEs in one spatial variable x and time t [63]. The PDEs that the function `pdepe` can solve must follow the general form

$$a_1\left(x,t,u,\frac{\partial u}{\partial x}\right)\frac{\partial u}{\partial t} = x^{-n}\frac{\partial}{\partial x}\left(x^n a_2\left(x,t,u,\frac{\partial u}{\partial x}\right)\right) + a_3\left(x,t,u,\frac{\partial u}{\partial x}\right) \tag{24}$$

Our model follows this form with $n = 0$, indicating rectangular coordinates for `pdepe`.

To enable code reuse, we wrote the model in MATLAB and shared the code including parameter values and documentation in an open-source software repository [64].

3. Results and Discussion

In this section, we present and analyze *in silico* experimental results in one dimension for three case studies of the model: (I) LOX is absent and has no effects on ECM and cancer cells (for all time steps: $l \equiv 0$, $f_{cl} \equiv 0$, $h \equiv 0$, and $g \equiv 0$); (II) LOX is present but not coupled to the haptotactic migration of cancer cells toward the cross-linked ECM fibers (for all time steps: $g \equiv 0$); (III) LOX is present and is coupled to the haptotactic migration of cancer cells. Note that for the entirety of the Section 3, we have dropped the "hat" notation for convenience. As described in Section 2.7, only dimensionless quantities are used in the model equations.

3.1. Case I: LOX Is Absent

In this case study, LOX is not present in the system, so $l \equiv 0$. This leads to no cross-linking of ECM collagen fibers, so $h \equiv 0$ and $f_{cl} \equiv 0$. Therefore, the term g that represents the haptotactic migration of cancer cells toward the cross-linked ECM collagen fibers is also turned off in the simulation, hence $g \equiv 0$. The system of PDEs is thus left with only three active species: c, f, and m.

The purpose of excluding LOX from the model in Case I is to validate our model before further exploration by comparing our results with those obtained from a highly cited published cancer invasion model [33]. The model in [33] included three PDEs for c, f, and m. Our results (not shown here) in Case I for the same three components combined with the same initial and boundary conditions used in [33] show the same results as the published model.

We set the initial condition as $m = 0$, deviating from [33], to consider the onset of MMP secretion from cancer cells. Figure 2 shows the spatial profiles of the tumor microenvironment at different dimensionless simulation times ($t = 0, 1, 10$, and 20). The results obtained for the population density of cancer cells capture a slow detachment of the cells away from the primary tumor mass (the left edge of the spatial domain) as time evolves. We also observe that ECM fiber concentration is low when and where MMP concentration is high. Such trends are expected due to the fact that MMP degrades and digests ECM collagen fibers.

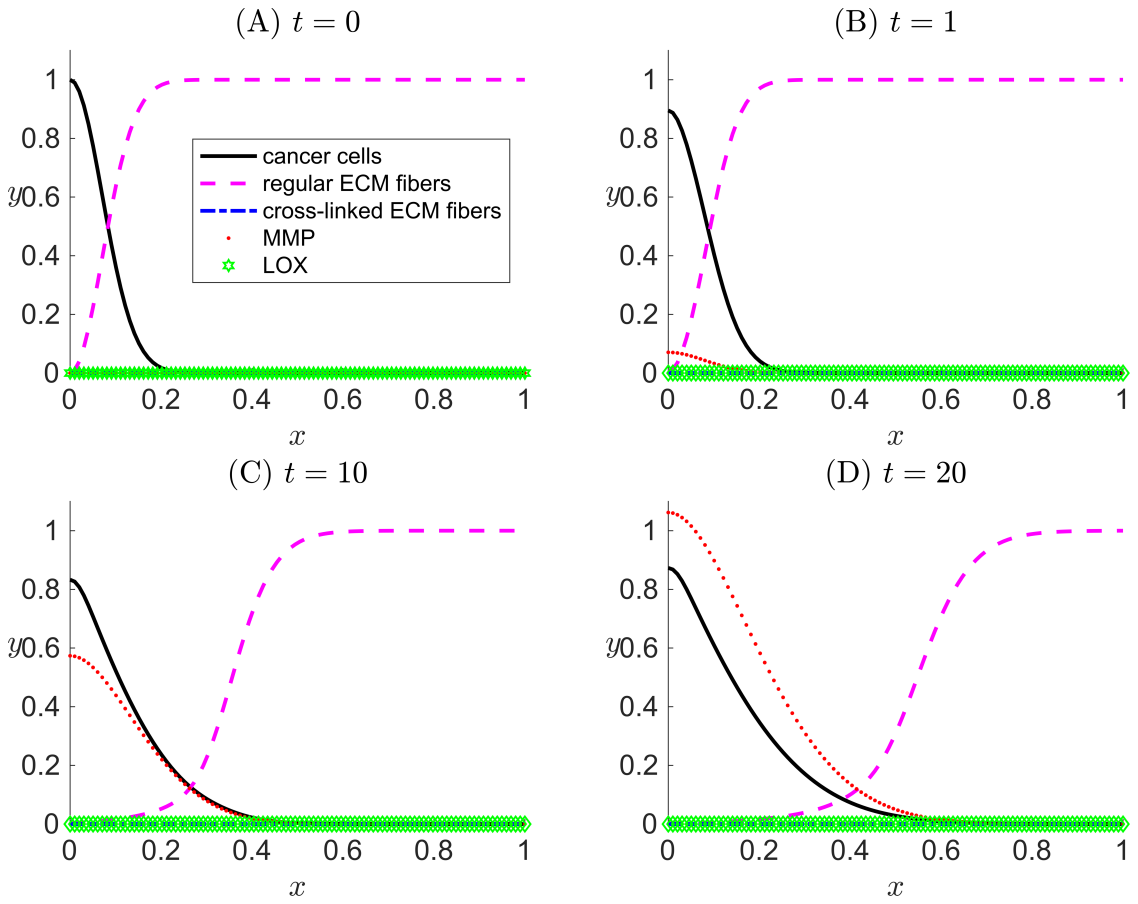

Figure 2. One-dimensional numerical results for Case I when there is zero concentration of LOX ($l \equiv 0$) and hence, zero cross-linked ECM collagen fibers f_{cl} in the system. Results are snapshots of the system dynamics at four simulation times: (**A**) $t = 0$, (**B**) $t = 1$, (**C**) $t = 10$, and (**D**) $t = 20$. For all four plots, the horizontal axis x indicates the dimensionless spatial position, and the vertical axis y indicates the dimensionless population density or concentration of the species listed in the legend.

3.2. Case II: LOX Is Present But Not Coupled to the Haptotactic Migration of Cancer Cells

In Case II, LOX l is included in the system. Since LOX is present, the rate of cross-linking of collagen fibers h is activated in the model. However, the haptotactic migration effect on the population density of cancer cells in (9) remains inactive in the simulation ($g \equiv 0$).

Our primary aim for the settings in Case II is to confirm that LOX can perform its main function on the ECM via the activation of h, which transforms regular collagen fibers to cross-linked fibers. Meanwhile, in the absence of the attraction of cancer cells toward the cross-linked fibers ($g \equiv 0$), the migration of cancer cells is only influenced by haptotactic migration toward the pristine collagen fibers f, which are present in lower concentrations compared with Case I since they can be reduced by cross-linking.

In Figure 3, the slow detachment of cancer cells away from the primary tumor mass and the effect of ECM degradation by MMP are captured in similar trends as in the Case I results and as in [33]. The main differences between the results of Cases I and II are the existence of the cross-linked ECM fibers and the f_{cl} dynamics. With h active and g inactive, the concentration of regular ECM fibers decreases more quickly and to a larger penetration distance due to cross-linking (compare the regular ECM fiber curve in Figure 3D with that in Figure 2D). This slightly reduces the cancer cell haptotactic driving force. Additionally, the volume occupancy fractions of other species are affected by f_{cl} in Case II.

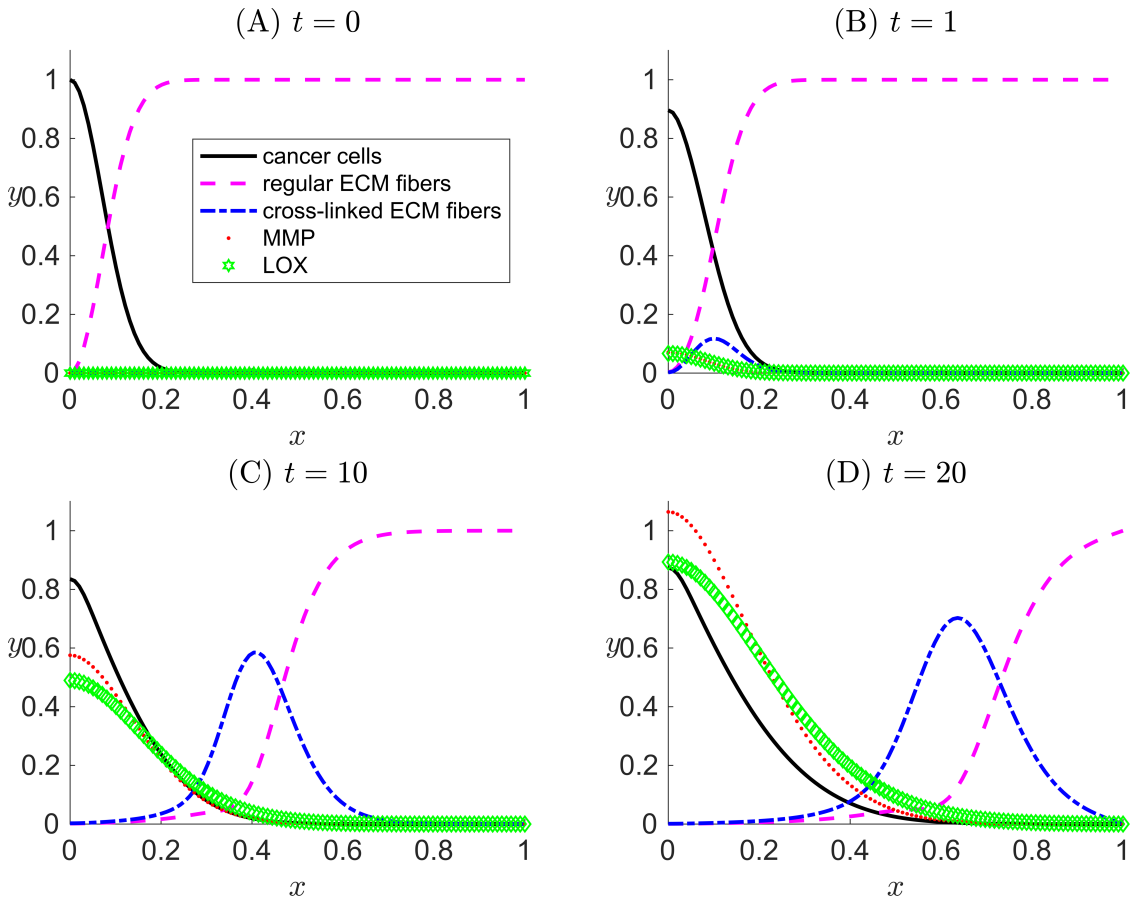

Figure 3. One-dimensional numerical results for Case II when LOX ($l \not\equiv 0$) and its effect only on the ECM collagen fibers and not on the cancer haptotaxis ($g \equiv 0$) are considered in the modeled system. The results are snapshots of the system dynamics at four simulation times: (**A**) $t = 0$, (**B**) $t = 1$, (**C**) $t = 10$, and (**D**) $t = 20$. For all four plots, the horizontal axis x indicates the dimensionless spatial position, and the vertical axis y indicates the dimensionless population density or concentration of the species listed in the legend.

3.3. Case III: LOX Is Present and Is Coupled to the Haptotactic Migration of Cancer Cells

In Case III, LOX is present in the system, and both the h and g terms are turned on in the model. In the simulation results (Figure 4), besides the recurrence of the expected phenomena from Cases I and II, a peak for cancer cells evolves over time away from the primary tumor ($x > 0.25$) (Figure 4C,D). The location of the peak of cancer cell population density corresponds to trailing the wave of cross-linked ECM fiber concentration. This suggests that cancer cells that have invaded the ECM via migration are clustered in the area where there is a high concentration of cross-linked ECM collagen fibers. Such behavior is the consequence of the haptotaxis effect caused by the directional motility of cancer cells toward the cross-linked ECM collagen fibers. Additionally, a smaller, secondary peak of regular ECM fibers appears to the left of the migrating cell front where conditions are favorable for the secretion of new regular ECM fibers.

Results of Case III have confirmed the capability of our new model to successfully implement the extended features to capture the cross-linking effect that LOX performs on the ECM. The results demonstrate how cross-linked fibers enhance the overall migration of cancer cells.

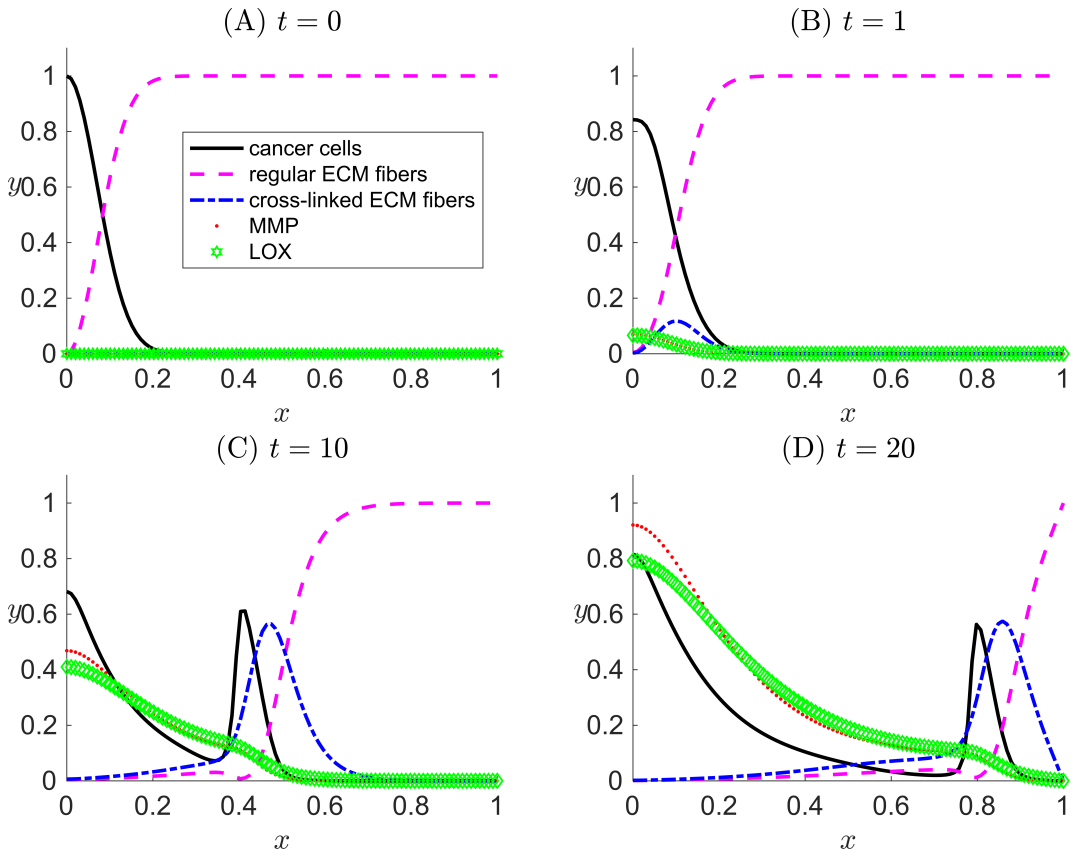

Figure 4. One-dimensional numerical results for Case III when LOX ($l \not\equiv 0$) and its effects both on the ECM collagen fibers and cancer cells motility are considered in the modeled system. Results are snapshots of the system dynamics at four simulation times: (**A**) $t = 0$, (**B**) $t = 1$, (**C**) $t = 10$, and (**D**) $t = 20$. For all four plots, the horizontal axis x indicates the dimensionless spatial position, and the vertical axis y indicates the dimensionless population density or concentration of the species listed in the legend.

3.4. Sensitivity Analysis

Local sensitivity assesses the impact of variations in each parameter on model outputs. The Case III conditions discussed in Section 3.3 are used. All of the dimensionless parameters listed in Table 2 are considered for perturbations in the local sensitivity analysis, except for $\hat{v}_1$, $\hat{v}_2$, and $\hat{v}_3$. The nominal values for the parameters are those listed in Table 2. The sensitivity analysis is conducted by varying each parameter, P_j, at a time by a small perturbation ΔP_j while keeping the other parameters fixed. We define the time-dependent local sensitivity index $S(t)$ as

$$S(t) = \frac{\max\limits_{x} |Y_i(P_j + \Delta P_j, P_{k\neq j}, x, t) - Y_i(P_j, P_{k\neq j}, x, t)|}{\Delta P_j} \tag{25}$$

where $Y_i(P, x, t)$ is the model prediction of the output variable i at position x and time t evaluated at parameter set P. The parameters and model equations are all dimensionless, so (25) is already normalized. Maximum deviations sorted with respect to x from the nominal case $Y_i(P_j, P_{k\neq j}, x, t)$ allow for the straightforward comparison of offsets over time due to parameter variations. ΔP_j is taken to be an increase of 10%.

We consider $S = 1$ to be a baseline threshold for categorizing parameter effects to be sensitive (i.e., a parameter is labeled "sensitive" if $S \geq 1$). In Figure 5, we show that, besides $\hat{D}_c$, $\hat{D}_m$, $\hat{D}_l$, $\hat{\alpha}_f$, and $\hat{\beta}_m$, the model outputs up to simulation time $t = 20$ are relatively insensitive to the other parameters. c is the output most sensitive to changes in input parameters, especially $\hat{D}_c$, $\hat{D}_m$, $\hat{D}_l$, $\hat{\alpha}_f$,

and $\hat{\beta}_m$ (Figure 5A). The two local sensitivity curves of parameters $\hat{\beta}_m$ and $\hat{\alpha}_f$ consistently overlap each other, indicating that any changes in these two parameters influence the model outputs with the same magnitudes over time (Figure 5A–C). Additionally, $\hat{\beta}_m$ and $\hat{\alpha}_f$ impact the model outputs of c, f, and f_{cl} more profoundly than others. The outputs of m and l are the most sensitive to the input parameters relating to chemical production by cancer cells $\hat{\beta}_m$ and $\hat{\beta}_l$, respectively (Figure 5D–E). From visual inspection of Figure 5F, it is clear that the maximum deviation from the baseline with respect to x occurs for $t = 20$ near $x = 0$ and that $\hat{\beta}_l$ is the most sensitive parameter for this scenario. The sensitivity index accounts for the same visual detection in a concise metric. The maximum with respect to x is considered because the peaks may shift in different parameter variation scenarios compared to the locations of the peaks in Figure 4, making it difficult to choose an x-position *a priori* at which the sensitivities can be fairly compared.

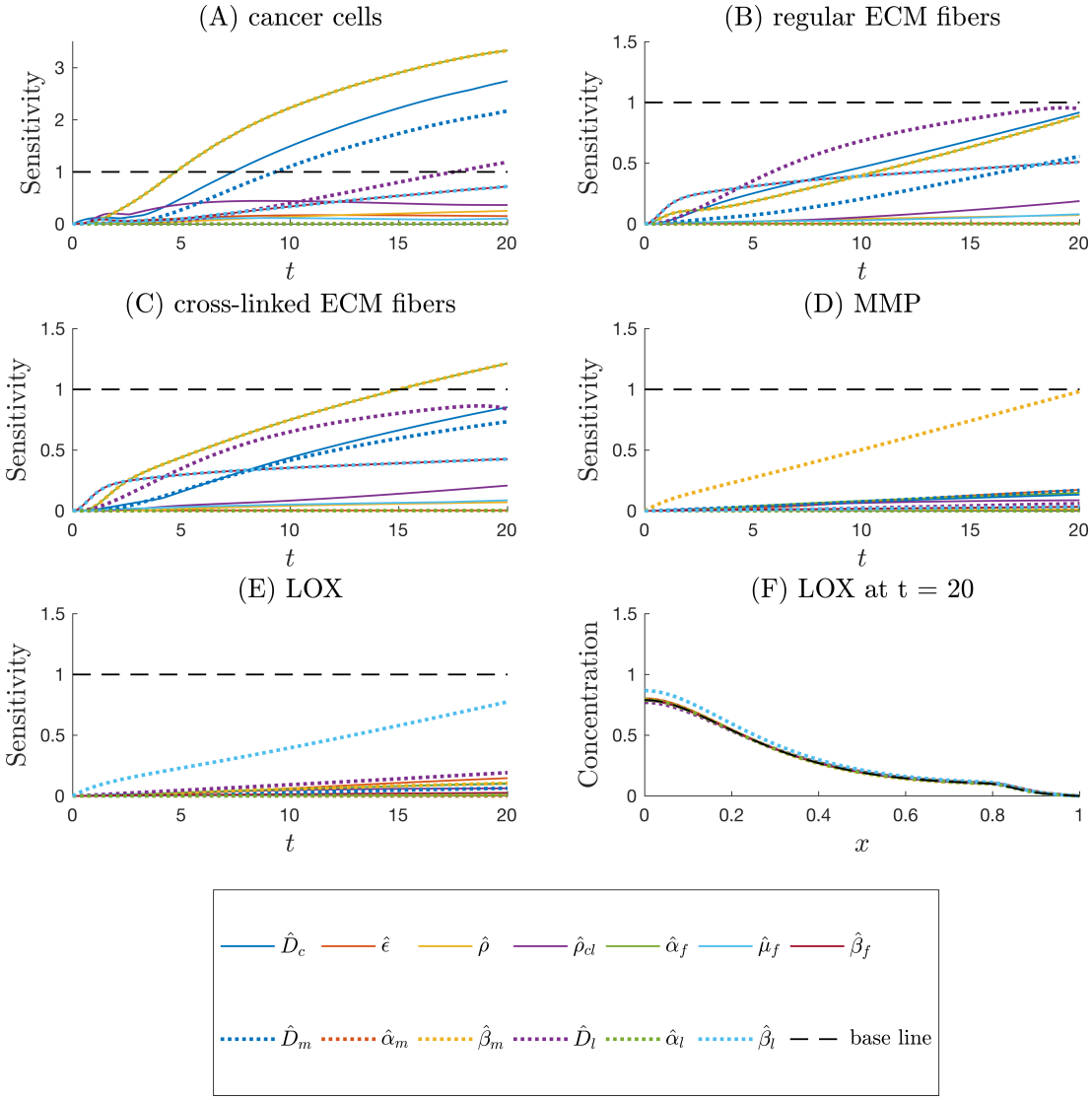

Figure 5. Local sensitivity index as a function of time assessing the impacts of 10% one-at-a-time increases in dimensionless parameters listed in Table 2 on the following model output variables: (**A**) the population density of cancer cells, (**B**) the concentration of regular ECM fibers, (**C**) the concentration of cross-linked ECM fibers, (**D**) the concentration of MMP, and (**E**) the concentration of LOX. (**F**) Model output profiles for concentration of LOX as a function of position x at at simulation time $t = 20$ corresponding to 10% changes in each parameter input. In (**A**–**E**), the baseline marks the threshold value of $S = 1$. In (**F**) the baseline marks the nominal LOX profile.

4. Conclusions

A model for reactions, diffusion, migration, and proliferation in the ECM undergoing dynamic remodeling has been proposed and analyzed. Case I, which only covers cancer cells, ECM density, and MMP concentration, has been verified and validated via comparison with a previous model [33]. The extended features of considering the enzyme LOX and its effect on ECM and cancer migration are successfully implemented in our new model demonstrated in Cases II and III. Simulation results of Case III have confirmed the capability of the model to capture the cross-linking effect that LOX performs on ECM and how cross-linked fibers enhance the overall migration of cancer cells. Based on the current model, an additional PDE could be included to potentially aid in optimizing drug transportation into the tumor through the remodeling ECM. This could result in a better understanding of the various processes that take place within the specific microenvironment and in the determination of tissue and/or chemical factors that may inhibit an administered drug from infiltrating the tumor [65]. Further, accounting for additional biological activities could allow for the model to represent a more complex and even more realistic system. Our model, in particular, has included the role of LOX in mathematical modeling of cancer migration and has raised the attention of the importance of this enzyme. The model provides a fundamental understanding that could facilitate predictions of new therapeutic development, for example, for inhibiting the effects of LOX or altering or slowing the remodeling rate of the ECM to slow down or prevent metastasis.

Author Contributions: Conceptualization: Y.T.N.E. and A.N.F.V.; formal analysis: Y.T.N.E. and A.N.F.V.; methodology: Y.T.N.E. and A.N.F.V.; software: Y.T.N.E.; supervision: A.N.F.V.; visualization: Y.T.N.E.; writing—original draft: Y.T.N.E.; writing—review and editing: Y.T.N.E. and A.N.F.V.

Acknowledgments: The authors would like to thank Oklahoma State University for startup support.

Conflicts of Interest: The authors declare no conflict of interest.

References

1. Cox, T.R.; Gartland, A.; Erler, J.T. Lysyl oxidase, a targetable secreted molecule involved in cancer metastasis. *Cancer Res.* **2016**, *76*, 188–192. [CrossRef] [PubMed]
2. Mendoza, M.; Khanna, C. Revisiting the seed and soil in cancer metastasis. *Int. J. Biochem. Cell Biol.* **2009**, *41*, 1452–1462. [CrossRef] [PubMed]
3. Bagley, R. *The Tumor Microenvironment*; Springer: New York, NY, USA, 2010.
4. Kahlert, C.; Kalluri, R. Exosomes in tumor microenvironment influence cancer progression and metastasis. *J. Mol. Med.* **2013**, *91*, 431–437. [CrossRef] [PubMed]
5. Wang, M.; Zhao, J.; Zhang, L.; Wei, F.; Lian, Y.; Wu, Y.; Gong, Z.; Zhang, S.; Zhou, J.; Cao, K.; et al. Role of tumor microenvironment in tumorigenesis. *J. Cancer* **2017**, *8*, 761–773. [CrossRef] [PubMed]
6. Keeratichamroen, S.; Lirdprapamongkol, K.; Svasti, J. Mechanism of ECM-induced dormancy and chemoresistance in A549 human lung carcinoma cells. *Oncol. Rep.* **2018**, *39*, 1765–1774. [CrossRef] [PubMed]
7. Kuhn, K. Basement membrane (type IV) collagen. *Matrix Biol.* **1995**, *14*, 439–445. [CrossRef]
8. Clark, A.G.; Vignjevic, D.M. Modes of cancer cell invasion and the role of the microenvironment. *Curr. Opin. Cell Biol.* **2015**, *36*, 13–22. [CrossRef] [PubMed]
9. Provenzano, P.P.; Eliceiri, K.W.; Campbell, J.M.; Inman, D.R.; White, J.G.; Keely, P.J. Collagen reorganization at the tumor-stromal interface facilitates local invasion. *BMC Med.* **2006**, *4*, 38. [CrossRef] [PubMed]
10. Lu, P.; Takai, K.; Weaver, V.M.; Werb, Z. Extracellular matrix degradation and remodeling in development and disease. *Cold Spring Harb. Perspect. Biol.* **2011**, *3*, a005058. [CrossRef] [PubMed]
11. Oudin, M.J.; Jonas, O.; Kosciuk, T.; Broye, L.C.; Guido, B.C.; Wyckoff, J.; Riquelme, D.; Lamar, J.M.; Asokan, S.B.; Whittaker, C.; et al. Tumor cell-driven extracellular matrix remodeling drives haptotaxis during metastatic progression. *Cancer Discov.* **2016**, *6*, 516–531. [CrossRef] [PubMed]
12. Bonnans, C.; Chou, J.; Werb, Z. Remodelling the extracellular matrix in development and disease. *Nat. Rev. Mol. Cell Biol.* **2014**, *15*, 786–801. [CrossRef] [PubMed]
13. Frantz, C.; Stewart, K.M.; Weaver, V.M. The extracellular matrix at a glance. *J. Cell Sci.* **2010**, *123*, 4195–4200. [CrossRef] [PubMed]

14. Yu, H.; Mouw, J.K.; Weaver, V.M. Forcing form and function: Biomechanical regulation of tumor evolution. *Trends Cell Biol.* **2011**, *21*, 47–56. [CrossRef] [PubMed]
15. Quaranta, V. Cell migration through extracellular matrix: Membrane-type metalloproteinases make the way. *J. Cell Biol.* **2000**, *149*, 1167–1170. [CrossRef] [PubMed]
16. Condeelis, J.; Segall, J.E. Intravital imaging of cell movement in tumours. *Nat. Rev. Cancer* **2003**, *3*, 921–930. [CrossRef] [PubMed]
17. Wyckoff, J.B.; Wang, Y.; Lin, E.Y.; Li, J.F.; Goswami, S.; Stanley, E.R.; Segall, J.E.; Pollard, J.W.; Condeelis, J. Direct visualization of macrophage-assisted tumor cell intravasation in mammary tumors. *Cancer Res.* **2007**, *67*, 2649–2656. [CrossRef] [PubMed]
18. Lu, P.; Weaver, V.M.; Werb, Z. The extracellular matrix: A dynamic niche in cancer progression. *J. Cell Biol.* **2012**, *196*, 395–406. [CrossRef] [PubMed]
19. Cawston, T.E.; Young, D.A. Proteinases involved in matrix turnover during cartilage and bone breakdown. *Cell Tissue Res.* **2010**, *339*, 221–235. [CrossRef] [PubMed]
20. Cathcart, J.; Pulkoski-Gross, A.; Cao, J. Targeting matrix metalloproteinases in cancer: Bringing new life to old ideas. *Genes Dis.* **2015**, *2*, 26–34. [CrossRef] [PubMed]
21. Gialeli, C.; Theocharis, A.D.; Karamanos, N.K. Roles of matrix metalloproteinases in cancer progression and their pharmacological targeting. *Cell Tissue Res.* **2010**, *339*, 221–235. [CrossRef] [PubMed]
22. Coussens, L.M.; Fingleton, B.; Matrisian, L.M. Matrix metalloproteinase inhibitors and cancer: Trials and tribulations. *Science* **2002**, *295*, 2387–2392. [CrossRef] [PubMed]
23. Fingleton, B. Chapter 36: MMP inhibitor clinical trials - the past, present, and future. In *The Cancer Degradome: Proteases and Cancer Biology*; Edwards, D., Hoyer-Hansen, G., Blasi, F., Sloane, B., Eds.; Springer: New York, NY, USA, 2008; pp. 759–785.
24. Smith-Mungo, L.I.; Kagan, H.M. Lysyl oxidase: Properties, regulation and multiple functions in biology. *Matrix Biol.* **1998**, *16*, 387–398. [CrossRef]
25. Egeblad, M.; Rasch, M.G.; Weaver, V.M. Dynamic interplay between the collagen scaffold and tumor evolution. *Curr. Opin. Cell Biol.* **2010**, *22*, 697–706. [CrossRef] [PubMed]
26. Rasmuson, A.; Andersson, B.; Olsson, L.; Andersson, R. *Mathematical Modeling in Chemical Engineering*; Cambridge University Press: Cambridge, UK, 2014.
27. Gatenby, R.A. Models of tumor-host interaction as competing populations: Implications for tumor biology and treatment. *J. Theor. Biol.* **1995**, *176*, 447–455. [CrossRef] [PubMed]
28. Gatenby, R.A.; Gawlinski, E.T. A reaction-diffusion model of cancer invasion. *Cancer Res.* **1996**, *56*, 5745–5753. [PubMed]
29. Orme, M.E.; Chaplain, M.A. A mathematical model of the first steps of tumour-related angiogenesis: Capillary sprout formation and secondary branching. *IMA J. Math. Appl. Med. Biol.* **1996**, *13*, 73–98. [CrossRef] [PubMed]
30. Perumapanani, A.J.; Sherratt, J.A.; Norbury, J.; Byrne, H.M. Biological inferences from a mathematical model for malignant invasion. *Invasion Metastasis* **1996**, *16*, 209–221.
31. Perumapanani, A.J.; Simmons, D.L.; Gearing, A.J.H.; Miller, K.M.; Ward, G.; Norbury, J.; Schneemann, M.; Sherratt, J.A. Extracellular matrix-mediated chemotaxis can impede cell migration. *Proc. Biol. Sci.* **1998**, *265*, 2347. [CrossRef]
32. Anderson, A.R.A.; Chaplain, M.A.J. Continuous and discrete mathematical models of tumor-induced angiogenesis. *Bull. Math. Biol.* **1998**, *60*, 857–899. [CrossRef] [PubMed]
33. Anderson, A.R.A.; Chaplain, M.A.J.; Newman, E.L.; Steele, R.J.C.; Thompson, A.M. Mathematical modelling of tumour invasion and metastasis. *J. Theor. Med.* **2000**, *2*, 129–154. [CrossRef]
34. Turner, S.; Sherratt, J.A. Intercellular adhesion and cancer invasion: A discrete simulation using the extended Potts model. *J. Theor. Biol.* **2002**, *16*, 85–100. [CrossRef] [PubMed]
35. Anderson, A.R.A. A hybrid mathematical model of solid tumour invasion: The importance of cell adhesion. *Math. Med. Biol.* **2005**, *22*, 163–186. [CrossRef] [PubMed]
36. Chaplain, M.A.J.; Lolas, G. Mathematical modeling of cancer cell invasion of tissue: The role of the urokinase plasminogen activation system. *Math. Models Methods Appl. Sci.* **2005**, *15*, 1685–1734. [CrossRef]
37. Chaplain, M.A.J.; Lolas, G. Mathematical modeling of cancer invasion of tissue: Dynamic heterogeneity. *Netw. Heterog. Media* **2006**, *1*, 399–439.

38. Frieboes, H.B.; Zheng, X.; Sun, C.; Tromberg, B.; Gatenby, R.; Cristini, V. An Integrated computational/experimental model of tumor invasion. *Cancer Res.* **2006**, *66*, 1597–1604. [CrossRef] [PubMed]
39. Hillen, T. M5 mesoscopic and macroscopic models for mesenchymal motion. *J. Math. Biol.* **2006**, *53*, 585–616. [CrossRef] [PubMed]
40. Gerisch, A.; Chaplain, M.A.J. Mathematical modelling of cancer cell invasion of tissue: Local and non-local models and the effect of adhesion. *J. Theor. Biol.* **2008**, *250*, 684–704. [CrossRef] [PubMed]
41. Ramis-Conde, I.; Drasdo, D.; Anderson, A.R.A.; Chaplain, M.A.J. Modeling the influence of the E-cadherin-β-catenin pathway in cancer cell invasion: A multiscale approach. *Biophys. J.* **2008**, *95*, 155–165. [CrossRef] [PubMed]
42. Anderson, A.; Rejniak, K.; Gerlee, P.; Quaranta, V. Microenvironment driven invasion: A multiscale multimodel investigation. *J. Math. Biol.* **2009**, *58*, 579–624. [CrossRef] [PubMed]
43. Poplawski, N.J.; Agero, U.; Gens, J.S.; Swat, M.; Glazier, J.A.; Anderson, A.R.A. Front instabilities and invasiveness of simulated avascular tumors. *Bull. Math. Biol.* **2009**, *71*, 1189–1227. [CrossRef] [PubMed]
44. Szymanska, Z.; Rodrigo, C.M.; Lachowicz, M.; Chaplain, M.A.J. Mathematical modelling of cancer invasion of tissue: The role and effect of nonlocal interactions. *Math. Models Methods Appl. Sci.* **2009**, *19*, 257–281. [CrossRef]
45. Painter, K.J. Modelling cell migration strategies in the extracellular matrix. *J. Math. Biol.* **2009**, *58*, 511–543. [CrossRef] [PubMed]
46. Painter, K.J.; Armstrong, N.A.; Sherratt, J.A. The impact of adhesion on cellular invasion processes in cancer and development. *J. Theor. Biol.* **2010**, *264*, 1057–1067. [CrossRef] [PubMed]
47. Andasari, V.; Gerisch, A.; Lolas, G.; South, A.P.; Chaplain, M.A.J. Mathematical modeling of cancer cell invasion of tissue: Biological insight from mathematical analysis and computational simulation. *J. Math. Biol.* **2011**, *63*, 141–171. [CrossRef] [PubMed]
48. Kolev, M.; Zubik-Kowal, B. Numerical solutions for a model of tissue invasion and migration of tumour cells. *Comput. Math. Methods Med.* **2011**, *2011*. [CrossRef] [PubMed]
49. Toma, A.; Mang, A.; Schuetz, T.A.; Becker, S.; Buzug, T.M. A novel method for simulating the extracellular matrix in models of tumour growth. *Comput. Math. Methods Med.* **2012**, *2012*. [CrossRef] [PubMed]
50. Deakin, N.E.; Chaplain, M.A.J. Mathematical modeling of cancer invasion: The role of membrane-bound matrix metalloproteinases. *Front. Oncol.* **2013**, *3*, 70. [CrossRef] [PubMed]
51. Evje, S. An integrative multiphase model for cancer cell migration under influence of physical cues from the microenvironment. *Chem. Eng. Sci.* **2017**, *165*, 240–259. [CrossRef]
52. Rejniak, K.A. *Systems Biology of Tumor Microenvironment: Quantitative Modeling and Simulations*; Springer International Publishing: Cham, Switzerland, 2016.
53. Kessenbrock, K.; Plaks, V.; Werb, Z. Matrix metalloproteinases: Regulators of the tumor microenvironment. *Cell* **2010**, *141*, 52–67. [CrossRef] [PubMed]
54. Pittayapruek, P.; Meephansan, J.; Prapapan, O.; Komine, M.; Ohtsuki, M. Role of matrix metalloproteinases in photoaging and photocarcinogenesis. *Int. J. Mol. Sci.* **2016**, *17*, 868. [CrossRef] [PubMed]
55. Brower, M.; Carney, D.N.; Oie, H.K.; Gazdar, A.F.; Minna, J.D. Growth of cell lines and clinical specimens of human non-small cell lung cancer in serum-free defined medium. *Cancer Res.* **1986**, *46*, 798–806. [PubMed]
56. Kremmer, T.; Palyi, I.; Daubner, D.; Boldizsar, M.; Vincze, B.; Paulik, E.; Sugar, J.; Pokorny, E.; Tury, E. Comparative studies on the polyamine metabolism and DFMO treatment of MCF-7 and MDA-MB-231 breast cancer cell lines and xenografts. *Anticancer Res.* **1991**, *11*, 1807–1813. [PubMed]
57. Limame, R.; Wouters, A.; Pauwels, B.; Fransen, E.; Peeters, M.; Lardon, F.; de Wever, O.; Pauwels, P. Comparative analysis of dynamic cell viability, migration and invasion assessments by novel real-time technology and classic endpoint assays. *PLoS ONE* **2012**, *7*, e46536. [CrossRef] [PubMed]
58. Oraiopoulou, M.E.; Tzamali, E.; Tzedakis, G.; Vakis, A.; Papamatheakis, J.; Sakkalis, V. In vitro/in silico study on the role of doubling time heterogeneity among primary glioblastoma cell lines. *BioMed Res. Int.* **2017**, *2017*, 8569328. [CrossRef] [PubMed]
59. Bray, D. *Cell Movements: From Molecules to Motility*; Garland Publishing: New York, NY, USA, 2001.
60. Collier, I.E.; Legant, W.; Marmer, B.; Lubman, O.; Saffarian, S.; Wakatsuki, T.; Elson, E.; Goldberg, G.I. Diffusion of MMPs on the surface of collagen fibrils: The mobile cell surface—Collagen substratum interface. *PLoS ONE* **2011**, *6*, 1–14. [CrossRef] [PubMed]

61. Terranova, V.P.; Diflorio, R.; Lyall, R.M.; Hic, S.; Friesel, R.; Maciag, T. Human endothelial cells are chemotactic to endothelial cell growth factor and heparin. *J. Cell Biol.* **1985**, *101*, 2330–2334. [CrossRef] [PubMed]
62. Kumar, S.; Das, A.; Barai, A.; Sen, S. MMP secretion rate and inter-invadopodia spacing collectively govern cancer invasiveness. *Biophys. J.* **2018**, *114*, 650–662. [CrossRef] [PubMed]
63. Higham, D.J. *MATLAB Guide*; Society for Industrial and Applied Mathematics: Philadelphia, PA, USA, 1992.
64. Nguyen Edalgo, Y.T.; Ford Versypt, A.N. MetastaticCancerECMRemodeling. 2018. Available online: http://github.com/ashleefv/MetastaticCancerECMRemodeling (accessed on 22 April 2018). [CrossRef]
65. Kim, M.J.; Gillies, R.J.; Rejniak, K.A. Current advances in mathematical modeling of anti-cancer drug penetration into tumor tissues. *Front. Oncol.* **2013**, *3*, 278. [CrossRef] [PubMed]